

Long-Term Erosion Rates of Forested Watersheds in Greater Battle Creek and Judd Creek

February 15, 2018

Prepared by:

Angus K. Moore and Darryl E. Granger Ph.D.
Department of Earth, Atmospheric, and Planetary Sciences
Purdue University
550 Stadium Mall Drive
West Lafayette, IN 47907



Funded by:

Research and Monitoring Program
Sierra Pacific Industries
P.O. Box 496028, Redding, CA 96409



ABOUT THE AUTHORS

Dr. Darryl Granger is a professor of geology in the Department of Earth, Atmospheric, and Planetary Sciences at Purdue University. He is a member of the Purdue Rare Isotope Measurement Laboratory (PRIME Lab), and a specialist in the application of cosmogenic nuclides to problems in geomorphology and in human evolution. Angus Moore is a Ph.D. student studying with Dr. Granger.

RECOMMENDED CITATION

Moore, A.; Granger, D. *Long-term Erosion Rates of Forested Watersheds in Greater Battle Creek and Judd Creek*; Sierra Pacific Industries: Redding, CA, 2018.

Available at: http://www.spi-ind.com/research/SPI_Purdue_EAPS_Report.pdf

1. INTRODUCTION

When evaluating the impacts of land use on erosion and sediment transport, it is important to compare modern rates of soil erosion with long-term rates in order to assess whether soils are being depleted or if modern erosion rates are within the geologic norm. Although modern rates can be estimated by sediment gauging and stream solute fluxes, long-term rates are more difficult to constrain. A relatively new technique for quantifying erosion rates over millennial timescales is based on the accumulation of cosmogenic nuclides in minerals exposed near the surface of the Earth. Over the last twenty years, this technique has become increasingly applied to establish background erosion rates against which annual or decadal sediment gauging records may be compared (Covault et al., 2013). The cosmogenic nuclide signal integrates over the time required to erode approximately 60 cm of rock, or 1.6 million metric tons km⁻² (Granger et al., 1996), and thus effectively captures the long-term average rate, while remaining insensitive to recent changes in the erosion rate due to land use or natural disturbances (Brown et al., 1998; Reusser et al., 2015; Schaller et al., 2001).

Comparisons between cosmogenic nuclide erosion rates and short-term sediment gauging records have been made at many locations around the globe, including forested watersheds in the western United States (Bierman et al., 2005; Ferrier et al., 2005; Kirchner et al., 2001). One of the main conclusions of this prior work is that sediment gauging often records a slower watershed erosion rate than cosmogenic nuclides, especially in small, mountainous catchments with little sediment storage (Covault et al., 2013; Kirchner et al., 2001). This is thought to be due to the episodicity of major erosional events triggered by extreme storms, wildfire, and other uncommon occurrences (Kirchner et al., 2001). Sediment gauging can accurately record the typical sediment flux, but may miss occasional extreme events that can dominate mass export from a watershed. If those extreme events are either not recorded or are discarded as outliers, then the gauging record will systematically underestimate the long-term sediment flux. Cosmogenic nuclides, in contrast, average over these short-term events and more closely approximate the background, geological erosion rate and thus can be used to assess sediment yields within the context of long-term landscape dynamics.

In this study, we determine long-term erosion rates with cosmogenic nuclides at nine watersheds or sub-watersheds upstream of continuous monitoring stations maintained by Sierra Pacific Industries (SPI) in the Greater Battle Creek area. These watersheds are developed on largely

andesitic volcanic rock that contains little to no quartz. This is significant because ^{10}Be in quartz, the standard cosmogenic nuclide/target mineral pair for determining erosion rates, cannot be applied in these watersheds. Instead, we obtained erosion rates with a recently established method that uses the cosmogenic nuclide ^{36}Cl in the mineral magnetite (Fe_3O_4). This method was developed and tested over the course of the last several years as part of a National Science Foundation (NSF)-funded project to expand the applicability of the cosmogenic nuclide erosion rate method to landscapes without quartz. The data presented herein represent the first application of this method beyond the initial testing and development phase.

This study was invited by SPI as a compliment to their long-term sediment-gauging record from continuous monitoring stations in the Greater Battle Creek area ([http://www.spi-ind.com/research/SPI Research and Monitoring QAPP.pdf](http://www.spi-ind.com/research/SPI%20Research%20and%20Monitoring%20QAPP.pdf)). SPI is aware that California's State Water Resources Control Board and Central Valley Regional Water Quality Control Board are providing funding through the Timber Regulation and Forest Restoration Program to conduct an assessment of these watersheds focusing on sediment and erosion. They requested that we provide this data in order to help them evaluate measured sediment yields against the background erosion rate. SPI provided project funding and logistical support for sample collection in California, while sample preparation, measurement, and analysis were conducted by the authors at Purdue University and the Purdue Rare Isotope Measurement (PRIME) Laboratory in West Lafayette, Indiana. The data from this project will contribute to a Ph.D. dissertation at Purdue University and portions were presented at the fall 2017 meeting of the American Geophysical Union and are in preparation for submission to *Earth and Planetary Science Letters*.

This report provides a brief review of cosmogenic nuclide systematics, describes study methods, and presents ^{36}Cl erosion rates for the Greater Battle Creek watersheds. The body of the report is organized into five sections. Section 2 provides background on cosmogenic nuclide methods, develops the theory needed to calculate erosion rates from measured cosmogenic nuclide concentrations, and discusses the various assumptions that are commonly made when interpreting measured concentrations as erosion rates. Section 3 discusses the geological characteristics of the study watersheds with special attention to the aspects that have bearing on the interpretation of cosmogenic erosion rates. Section 4 presents sample collection, preparation, and measurement procedures. Section 5 gives the erosion rate results, and Section 6 interprets the erosion rates within the context of individual watersheds.

2. THEORETICAL BACKGROUND

Cosmogenic nuclides are produced through nuclear reactions between secondary cosmic ray particles and the nuclei of elements in mineral grains. Fundamentally, the cosmogenic nuclide inventory of a sample is related to the erosion rate because the cosmic ray flux, and therefore the production rate of cosmogenic nuclides, declines with depth to an almost negligible level a few meters below the ground surface. The concentration of a cosmogenic nuclide in a mineral grain eroding from a single point on the landscape will therefore reflect the speed with which erosion exhumed that grain through the upper few meters of the Earth's crust (Lal, 1991). Likewise, the concentration in a sample of stream sediment containing a large number of individual mineral grains originating from many points across a watershed will provide an estimate of the spatially averaged erosion rate upstream from the collection point (Granger et al., 1996). This allows a single analysis of well-mixed stream sediment to furnish an estimate of the erosion rate in a whole hydrologic catchment provided several assumptions are met (see Section 2.3).

2.1 Production of Cosmogenic Nuclides

Interaction of galactic cosmic rays with the Earth's atmosphere produces a cascade of secondary cosmic ray particles that is dominated by neutrons near the Earth's surface. Production of ^{36}Cl in magnetite occurs through two different types of cosmic ray induced nuclear reaction: spallation and low-energy neutron capture. These reactions have different characteristic depth-attenuation scales, and because the cosmogenic nuclide inventory of an eroding sample reflects the production rate integrated through the sample's exhumation path, both must be taken into consideration.

Spallation on Fe dominates the production of ^{36}Cl in magnetite. In a spallation reaction, a high-energy neutron impacts and fragments the nucleus of a target element, producing a product nuclide with a lower atomic mass. The production rate of cosmogenic nuclides by spallation declines with depth below the surface according to an exponential decay law, as cosmic rays are increasingly shielded by overlying rock or soil:

$$P_s(z) = P_s(0)e^{-z/\Lambda_f} \quad (1)$$

where $P_s(z)$ is the spallogenic production rate of a cosmogenic nuclide (atoms $\text{g}^{-1} \text{yr}^{-1}$) at some mass-depth z (g cm^{-2}), $P_s(0)$ is the surface production rate, and Λ_f is related to the mean free path of high energy neutrons (g cm^{-2}) (Lal, 1991).

^{36}Cl may also be produced through thermal and epithermal (low-energy) neutron capture. This reaction converts common ^{35}Cl into cosmogenic ^{36}Cl and is an important production pathway in magnetite samples with more than a few parts per million native chloride. Low-energy neutrons are produced mostly by moderation of high-energy cosmic ray neutrons. They behave diffusively and their flux in the subsurface is regulated by the neutron moderation and absorption properties of the surrounding rock or soil. As such, it is highly sensitive to the presence of trace quantities of elements that are especially effective neutron absorbers or moderators such as B or H. ^{36}Cl production by low-energy neutron capture may be approximated using a series of five exponential terms:

$$P_n(z) = \left[k_1 e^{-\frac{z}{\Lambda_f}} + k_2 e^{-\frac{z}{L_{eth}}} \right]_{eth} + \left[k_3 e^{-\frac{z}{\Lambda_f}} + k_4 e^{-\frac{z}{L_{eth}}} + k_5 e^{-\frac{z}{L_{th}}} \right]_{th} \quad (2)$$

where subscripts *eth* and *th* denote epithermal and thermal, L_{eth} and L_{th} are the diffusion lengths of epithermal and thermal neutrons (g cm^{-2}), and k_1 , k_2 , k_3 , k_4 , and k_5 are constants ($\text{atoms g}^{-1} \text{yr}^{-1}$) calculated from nuclear physics parameters and the composition of a sample's environment. Terms k_2 , k_4 , and k_5 account for diffusive neutron "leakage" and may take a negative sign (Liu et al., 1994; Marrero et al., 2015; Phillips et al., 2001).

2.2 Determining Erosion Rates

Assuming that mineral grains approach the surface at a constant denudation rate, the concentration of a cosmogenic nuclide in a sample experiencing erosion will reflect the production rate integrated across the exhumation path, less any radioactive decay. In steady state, this is described by:

$$N = \sum_i \frac{P_i(0)}{\lambda + E/\Lambda_i} \quad (3)$$

where N is the concentration of the nuclide (atoms g^{-1}), E is the erosion rate (g cm^{-2}), $P_i(0)$ is the production rate at the surface by production reaction i ($\text{atoms g}^{-1} \text{yr}^{-1}$), Λ_i is the effective mean free path or penetration length of the cosmic radiation responsible for production reaction i (g cm^{-2}), and λ is the decay constant of the nuclide of interest (Granger and Riebe, 2014). The erosion rate in this expression (E) is equivalent to the physical erosion rate and hence directly comparable to the sediment-gauging erosion rate only when chemical weathering is negligible. The presence of

chemical weathering introduces a complication that is considered further in Section 2.3.4. When λ is small relative to E/Λ_i decay may be ignored and eqn. 4 can be rearranged to produce:

$$E = \sum_i \frac{P_i(0)\Lambda_i}{N} \quad (4)$$

This expression is the basis for most published cosmogenic nuclide erosion rate calculations. Considering all production mechanisms, the erosion rate from a measured ^{36}Cl concentration is given by:

$$E = \frac{P_{sp}\Lambda_f}{N_{36}} + \frac{k_1\Lambda_f}{N_{36}} + \frac{k_2L_{eth}}{N_{36}} + \frac{k_3\Lambda_f}{N_{36}} + \frac{k_4L_{eth}}{N_{36}} + \frac{k_5L_{th}}{N_{36}} \quad (5)$$

We employ eqn. 5 to calculate the watershed erosion rates in this study. We also determine erosion rates using eqn. 3 summing over the same production mechanisms shown in eqn. 5, but incorporating the radioactive decay term in order to assess the impact of decay on the erosion rate results.

2.3 Complications

2.3.1 Disequilibrium

Eqns. 3 and 5 assume that erosion is in steady-state, implying that nuclide production and removal by erosion balance such that the nuclide concentration does not change with time. This model is not strictly valid where portions of a watershed are covered by young alluvium or glacial deposits on which equilibrium is not yet established (Wittmann et al., 2007). In this case, the nuclide concentration will be lower than the equilibrium concentration and the erosion rate will be biased towards a value that is too high. The same problem occurs in catchments where land sliding mobilizes deep-seated material with a low nuclide concentration and where deep glacial scouring exhumed fresh rock not previously exposed to cosmic radiation (Norton et al., 2010). Eqns. 3 and 5 also assume that the sample contained no cosmogenic nuclides when buried deep in the earth and shielded from cosmic radiation. This may not be the case for glacial and alluvial materials that experienced exposure to cosmic radiation prior to mobilization and re-deposition by ice or water. These “inherited” nuclides will tend to skew the erosion rate towards a value that is too low.

2.3.2 Heterogeneous Target Mineral Distribution

Another important assumption required by eqns. 3 and 5 is that the target mineral is distributed uniformly within the watershed. This is a valid assumption where the watershed of interest is developed on a single, uniform lithology, but is invalid for the watersheds considered in this study that are underlain by heterogeneous volcanic and alluvial parent materials. In this case, the erosion rate determined from cosmogenic nuclides will represent the average of the erosion rates in the various sub-catchments weighted by the relative concentration of the target mineral in the parent material of each sub-catchment (Carretier et al., 2015; Safran et al., 2005). The importance of the target mineral distribution to the catchment-averaged erosion rate depends on how much the erosion rate and target mineral concentrations vary between sub-catchments. In the limit where a target mineral is present in only a portion of the watershed and absent elsewhere, the erosion rate from the target mineral will reflect the erosion rate in the source area alone, which may differ appreciably from the true catchment-averaged rate.

2.3.3 Chemical Weathering

Chemical weathering may also present a significant complication. A conceptual model widely used in cosmogenic nuclide studies to account for chemical weathering divides the subsurface into a well-mixed soil (which is continuously homogenized by tree throw, burrowing, creep, etc.) and subsoil which remains unmixed and retains the original structure of the parent material. The soil mass is considered to be in steady state, with soil production balancing soil erosion. In this model, eqns. 3 and 5 are only valid in the absence of chemical weathering. Where weathering is important, cosmogenic nuclide accumulation in a weathering-resistant target mineral (such as magnetite) in the subsoil will be sensitive to mass loss by both physical and chemical weathering in the overlying soil. This means that eqns. 3 and 5 will systematically over-estimate the physical erosion rate. A correction for this bias can be developed from measurements of insoluble element enrichment across the soil/subsoil interface; however, as we lack this data we omit such a correction from this analysis. The resulting bias in the erosion rates is unlikely to exceed 10-20%.

3. WATERSHED GEOLOGY

The geological context of a watershed is important because it has bearing on several of the assumptions discussed above. The Greater Battle Creek watersheds are developed on volcanic rocks of mostly intermediate compositions but varying ages. Figure I contains a map of the study watersheds including the location of sampling sites as well as simplified geology. The geology is

taken from Jennings et al. (1977) and is available from the California Geological Survey. It provides a level of detail sufficient to highlight the distribution of andesitic bedrock vs. unconsolidated deposits within each watershed, but omits much of the local variation in bedrock lithology. For a more detailed geological map of the southern Cascades study sites see Clynne and Muffler (2010).

3.1 Battle Creek Tributaries

The study watersheds that are tributaries of Battle Creek are located west of Mt. Lassen in Shasta and Tehama Cos., California. From north to south these are Bailey Creek, Canyon Creek, North Digger Creek, and South Digger Creek. The bedrock in these watersheds consists of volcanic material that ranges from basaltic andesite through rhyolite in composition and is dominated by dacite and andesite. The rocks are chiefly mid-Pleistocene in age, with radiometric dates ranging from ca. 300-800 ka, and record activity of the Lassen Volcanic Center (Clynne & Mussler, 2010). The magnetic sediment collected from these watersheds consisted of both individual magnetite grains as well as lithic fragments with finely disseminated magnetite. All magnetite samples contained high concentrations of Ti (8-15%). Large portions of Bailey Creek and smaller areas of the other three watersheds are covered by till, glacial outwash, and alluvium. In particular, there are well-preserved late-Pleistocene moraine complexes in the upper reaches of Bailey Creek and both North and South Digger Creeks.

3.2 Judd Creek

Judd Creek is located in Tehama Co., California, approximately 15 km south of the Battle Creek tributaries. Sediment samples were collected at five sites along the course of the creek. From highest to lowest elevation these are numbered Judd1 through Judd5. Judd Creek is developed on early Pleistocene (ca. 2,100-2,150 ka) dacite and basaltic andesite erupted from the Maidu Volcanic Center. This was located southwest of the present Lassen Volcanic Center which it predates in age. The Judd Creek watershed, like the Battle Creek tributaries, is long and narrow, stretching more than 13 km in length while never exceeding about 2.5 km in width. Judd Creek encompasses a wet, alluviated meadow greater than 1 km in length along the watercourse between the Judd1 and Judd2 sampling sites. While crossing the meadow, the active channel of Judd Creek loses grade and becomes distributary and anastomosing, suggesting that the meadow serves as a sediment sink and traps coarse-grained sediment and heavy minerals (including magnetite) sourced from upstream. The magnetite from Judd Creek sediment contained between 8 and 12 wt. % Ti.

Table I. Watershed Data

Site	Latitude (°N)*	Longitude (°E)*	Mean El. (m asl)	Area (km ²)
Bailey Canyon	██████	██████	1772	61.68
North Digger	██████	██████	1830	28.12
South Digger	██████	██████	1757	25.04
Judd1	██████	██████	1478	8.59
Judd2	██████	██████	1397	12.02
Judd3	██████	██████	1362	14.19
Judd4	██████	██████	1319	16.56
Judd5	██████	██████	1307	17.24

* Proprietary information withheld at the request of Sierra Pacific Industries

4. METHODS

4.1 Sample Collection

Magnetite-bearing magnetic sediment was collected using rare-earth magnets encased in a plastic tube. The tube was dragged along the stream bed and through sandy areas until covered in magnetic sediment. This was scraped from the rod into a sample bag and the dragging and scraping processes repeated until a 1-2-kg sample was obtained. Both bulk and magnetic samples were collected from more than three locations along the stream bed in order to maximize the likelihood of obtaining a well-mixed sample. Care was taken to avoid sampling beneath or immediately downstream of cut-banks, which may furnish sediment directly to the channel without the chance for homogenization by mixing during transport.

4.2 Mineral Separation

Magnetite separates were obtained from the magnetic sediment samples using separation procedures that exploit magnetite's strong ferrimagnetism. In brief, the samples were crushed in a shatter-box and then concentrated using rare-earth hand magnets to obtain separates consisting of ~98-99% Fe-Ti oxides. These were then ground for 90 minutes on an oscillatory shaker with zirconia grinding balls to reduce grain size to the 1-10- μ range and destroy fluid inclusions that may contain chloride. This step is necessary to lower sample chloride content which simplifies ³⁶Cl production systematics by reducing the importance of the often ambiguous low-energy neutron capture production pathway on ³⁵Cl (see Section 2.1). Grinding was followed by a dithionite-citrate-bicarbonate extraction to remove secondary iron-oxides and then two leaches in 1% HF/HNO₃ to

dissolve residual silicates and clean grain surfaces. Sample preparation for dissolution was finished with three cycles of leaching in 1% ammonium hydroxide and copious washing in high-purity water to remove any surface adsorbed chloride.

4.3 Chemical Preparation

The clean magnetite separates were spiked with ^{35}Cl enriched carrier (99.65% ^{35}Cl , ICON isotopes) and dissolved in high purity oxalic acid. Dissolution was allowed to progress for one week at approximately 50 °C. At the end of the week, the remaining solids were centrifuged off and the mineral residue was isolated, washed, dried, and massed. This residual mass was subtracted from the initial mass to yield the mass of dissolved sample. After removal of the solids, the solution was acidified with HNO_3 and the Cl precipitated as AgCl by the addition of an excess of AgNO_3 . The AgCl precipitate was recovered by centrifugation, complexed with ammonium hydroxide, and purified by anion chromatography. The pure AgCl product was centrifuged into a pellet, dried, and loaded into a copper cathode filled with AgBr for measurement by accelerator mass spectrometry (AMS).

4.4 Analytical Measurements and Results

4.4.1 AMS Measurement of ^{36}Cl

$^{36}\text{Cl}/\text{Cl}_{\text{Total}}$ ratios were measured on the PRIME Lab AMS at Purdue University. ^{36}Cl measurements were normalized against the Sharma et al. (1990) ^{36}Cl standard. ^{36}Cl concentrations were calculated from the spike and sample masses and the measured isotope ratios. All calculated ^{36}Cl concentrations are reported in Table II.

4.4.2 Target Chemistry

Magnetite may be subject to extensive substitution of various cations for Fe. Possible substituents include target elements for ^{36}Cl production such as K, Ca, and especially Ti. An accurate assessment of the ^{36}Cl production rate in a magnetite sample therefore requires the determination of sample bulk chemistry. This was measured on an approximately 50 mg split of each clean magnetite separate that was taken prior to sample dissolution and dissolved separately in pyro-phosphoric acid. Once in solution, the sample was diluted with HNO_3 and analyzed for K, Ca, and Ti on an inductively coupled plasma-optical emission spectrometer. Fe concentrations were determined from sample stoichiometry assuming K, Ca, and Ti as the only substituting cations. ^{36}Cl may also be produced by low-energy neutron capture on ^{35}Cl . This requires measurement of the stable chloride concentration in each sample. This was accomplished through an isotope dilution approach

assuming mixing of the ^{35}Cl -enriched spike with stable chloride with an invariant $^{35}\text{Cl}/^{37}\text{Cl}$ ratio (Desilets, 2006). ^{35}Cl and ^{37}Cl currents were measured during AMS analysis and stable chloride concentrations were calculated from the ^{35}Cl to ^{37}Cl ratio. Sample chloride concentrations were blank-corrected to account for stable chloride introduced by the chemical reagents used in sample preparation. The concentrations of ^{36}Cl target elements in each sample are given in Table II.

Table II. Measurement Results

Site	$[^{36}\text{Cl}]$ (atoms g^{-1})	Uncert.	ppm Cl	Uncert.	ppm K	ppm Ca	wt. % Ti	wt. % Fe
Bailey Canyon	221000	9000	18	1	49	808	12	58
North Digger	278000	8000	29	1	4	436	15	55
South Digger	258000	13000	24	2	34	573	8	63
Judd1	230000	6000	21	0	45	544	9	62
Judd2	174000	6000	8	1	63	1281	11	60
Judd3	395000	11000	17	1	127	1148	11	60
Judd4	327000	16000	10	3	49	808	12	58
Judd5	341000	18000	4	3	49	808	12	58
Judd5	271000	12000	4	1	34	573	8	63

5. ANALYSIS

5.1 Production Parameters

The most important ^{36}Cl production mechanism in magnetite is spallation on Fe. For this reaction a reference production rate of 1.72 ± 0.05 atoms ^{36}Cl g-Fe^{-1} yr^{-1} was used (Moore, 2017). The reference production rate of ^{36}Cl production from Ti was approximated as 3.98 atoms ^{36}Cl g-Ti^{-1} yr^{-1} from the Fe production rate and the Fe/Ti production ratio estimated from nuclear reaction cross sections (Masarik, 2002). Reference spallation production rates for ^{36}Cl from K and Ca were adopted from Marrero et al., (2015). ^{36}Cl production by low-energy neutron capture is difficult to constrain because it is dependent on the chemical composition of the sample's environment. The composition of the largely andesitic rocks underlying the study watersheds was approximated with data compiled from several sources. Major element compositions for andesite were taken from Parker (1967) and trace elements from measurements of stream sediment geochemistry near the study sites available through the United States Geological Survey (USGS) and the National Geochemical Survey (NGS) database. Mean soil carbon and nitrogen values for soils in the continental United States were used (Shacklette and Boerngen, 1984), while concentrations of important neutron absorbers not reported in the NGS data (e.g. B or Gd) were estimated.

In this analysis, special consideration must be given to hydrogen, which is a very effective neutron moderator and thus plays a critical role in regulating the low-energy neutron flux. Hydrogen may be present as pore water, adsorbed water, snow, and structural water in clays, hydrous primary minerals, and soil organic matter. Approximating the contributions of each of these sources, soils were estimated to contain hydrogen equivalent to 25 wt. % water. Bulk densities of 0.9 and 1.3 g cm⁻³ are used for soils developed on andesite and granitic rock, respectively. Each was adjusted upwards by 0.2 g cm⁻³ to account for pore water. Each of the constants in eqn. 2 were calculated using the measured sample chloride contents and these estimates of watershed chemical composition following the theory developed by Phillips et al. (2001) as implemented by Schimmelpfennig et al. (2009).

5.1.1 Production Rate Scaling

Cosmogenic nuclide production rates vary systematically with elevation and geomagnetic latitude, and so require scaling to individual study sites. In this analysis, reference production rates are scaled using the Lal/Stone (2000) model. Watershed-averaged scaling factors were determined by dividing each watershed into 1-m elevation bins, computing the production rate at each elevation bin, and then taking the spatially weighted average. Snow and biomass may also influence the production rate by shielding the ground surface from incident cosmic radiation. While likely reducing production of ³⁶Cl by 5-10% in the study watersheds, we lack data on mean snow depth and biomass density, and so omit corrections for shielding in this analysis.

Table III. Parameters*

Site	Λ_f	P-spCl	k1	k2	k3	k4	k5	L1	L2
Bailey Canyon	155.31	6.251	0.181	0.302	2.027	-2.780	-1.095	1.539	8.110
North Digger	154.86	5.354	0.200	0.333	2.241	-3.074	-1.211	1.539	8.110
South Digger	155.43	5.989	0.210	0.351	2.359	-3.236	-1.275	1.539	8.110
Judd1	155.28	5.264	0.235	0.393	2.640	-3.621	-1.426	1.539	8.110
Judd2	154.36	4.850	0.075	0.126	0.844	-1.157	-0.456	1.539	8.110
Judd3	154.38	4.595	0.096	0.161	1.080	-1.481	-0.584	1.539	8.110
Judd4	154.48	4.496	0.064	0.107	0.720	-0.987	-0.389	1.539	8.110
Judd5	154.55	4.360	0.031	0.053	0.353	-0.484	-0.191	1.539	8.110
Judd5	154.72	4.042	0.030	0.051	0.340	-0.466	-0.184	1.539	8.110

* Λ_f is in g cm⁻², P_{sp} is in units of atoms g⁻¹ yr⁻¹, and the diffusion and attenuation lengths g cm⁻² yr⁻¹.

5.2 Erosion Rates

Calculated erosion rates and associated uncertainties are shown in Table IV. Raw erosion rates from magnetite range from 21 to 62 tons km⁻² yr⁻¹. Both internal and external uncertainties are quoted in Table IV. The former reflect only AMS analytical uncertainties, whereas the latter also include uncertainty in the reference spallation production rates and a 25% uncertainty assigned to production by neutron capture in order to encapsulate the large, unquantifiable uncertainty in average watershed composition. The external uncertainty provides a more comprehensive estimate of uncertainty and, in that respect, is more appropriate to consider when comparing cosmogenic erosion rates to sediment-gauging data. To evaluate the influence of radioactive decay on the calculated erosion rates, eqn. 4 was solved iteratively and the results are also presented in Table IV under decay-corrected E₃₆.

5.3 Averaging Timescales

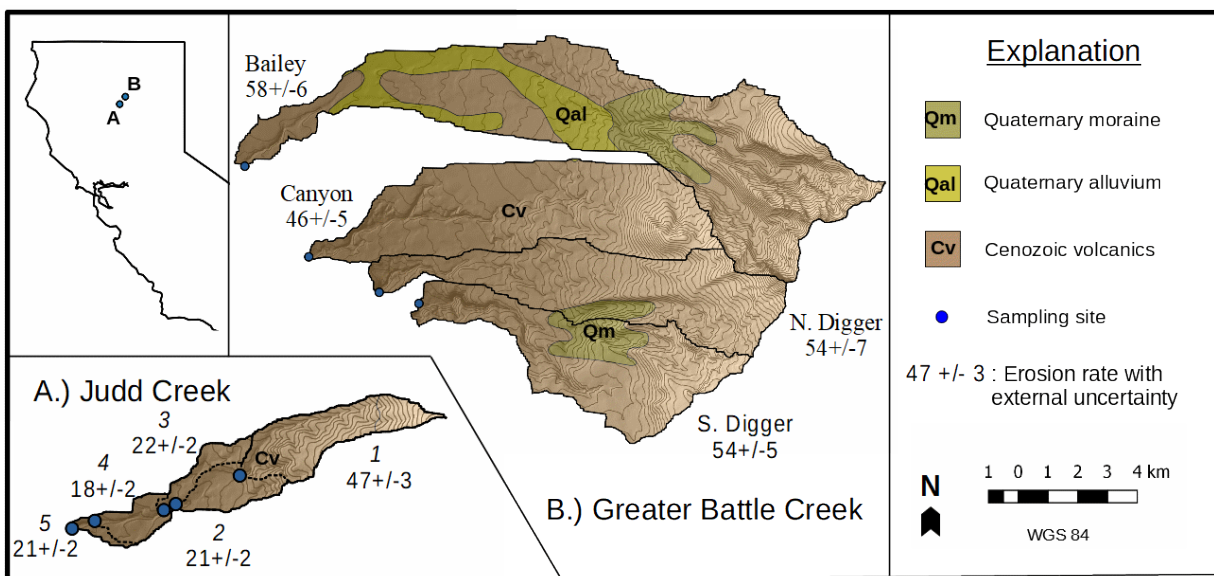
The averaging time of an erosion rate from cosmogenic nuclides is proportional to the amount of time required to erode a mass per unit area equivalent to the mean free path of cosmic radiation. Apparent averaging timescales for these watersheds are shown in Table IV and range from a low of 25,300 years for Bailey Creek to a high of 72,800 years for Judd4. The averaging time of erosion rates at all watersheds extends into the last glacial period and may partly reflect a different background rate of erosion which prevailed under a cooler climatic regime. However, the long-averaging timescale also suggests that the data are insensitive to changes in erosion rate due to land use in California since the 19th century.

Table IV. Erosion Rates*

Site	Erosion Rate	Internal Uncert.	External Uncert.	Decay corrected	Averaging Time (yr)
Bailey	61.5	2.4	5.6	57.7	25300
Rock	49.1	1.4	5.4	45.5	31500
North Digger	57.1	2.8	6.5	53.5	27200
South Digger	57.4	1.5	5.4	53.8	27000
Judd1	50.4	1.8	3.0	46.8	30700
Judd2	25.0	0.7	2.1	21.4	61800
Judd3	25.7	1.2	2.4	22.1	60100
Judd4	21.2	1.1	1.9	17.6	72800
Judd5	25.0	1.1	1.5	21.4	61800

* Erosion rate units are in metric tons km⁻² yr⁻¹.

Figure I. Map of Study Watersheds with ^{36}Cl -based Erosion Rates ($\text{tons km}^{-2} \text{yr}^{-1}$)



6. DISCUSSION

6.1 Battle Creek Tributaries

The Battle Creek tributary watersheds are estimated to be eroding at between 46 and 58 $\text{tons km}^{-2} \text{yr}^{-1}$ (decay corrected). However, as noted in the watershed descriptions, alluvium and glacial deposits are prevalent at these sites. Inherited cosmogenic nuclides will skew the erosion rate towards a value that is too low, while failure to re-establish equilibrium since de-glaciation or alluvium deposition between nuclide production and loss through erosion will bias erosion rates in the opposite direction. The size of this bias decreases with time since de-glaciation or deposition and with an increasing erosion rate. Assuming that the glaciated portions of the watersheds were exposed following the retreat of Tioga 3 ice at approximately 17,000 BP (Phillips, 2016) and that the actual erosion rate is 60 $\text{tons km}^{-2} \text{yr}^{-1}$, the erosion rate calculated for the glaciated area will be over-estimated by about 50%. The bias will have a similar magnitude in the alluviated parts of the catchments if the alluvium is primarily outwash associated with Tioga ice. However, if the alluvium substantially pre-dates the Tioga glaciation, the bias should be minor. As only portions of the Battle Creek tributary watersheds were glaciated or alluviated, and as some inherited cosmogenic nuclides are likely present in both the alluvium and glacial deposits, the net bias should not exceed 10-20% in any of the study watersheds.

6.2 Judd Creek

The ^{36}Cl -based erosion rates along Judd Creek exhibit a major discontinuity between Judd1 and Judd2 across which the rate drops by a more than a factor of two. The erosion rate then remains effectively constant from Judd2 through the bottom of the series. The most likely explanation for this pattern is that sediment sourced from above Judd1 is trapped in the meadow that lies between Judd1 and Judd2. In this meadow, Judd Creek loses grade and, consequently, much of its capacity to transport coarse grained sediment and heavy minerals such as magnetite. If sediment carrying the erosion rate signal from above the meadow is trapped, then the erosion rates determined at the sampling sites below the meadow may reflect only the average rate between the sampling site and the base of the meadow, and not the average in the whole Judd Creek watershed.

6.3 Independent Constraints on the Long-term Erosion Rate

This study represents the first application of a new method to determine cosmogenic erosion rates in watersheds developed on volcanic rock without quartz, which precludes comparison to other cosmogenic nuclide work. An effective and widely used non-cosmogenic method to determine long-term erosion rates on volcanic landscapes involves comparing present topography with reconstructions of the original volcanic form (Ferrier et al., 2013; Ruxton and McDougall, 1967). Karátson et al. (2012) determined long-term denudation rates in this way for 33 andesitic stratovolcanoes in the Central Andean Volcanic Zone and produced values ranging from 7-112 m/m.y. ($\sim 18\text{-}280 \text{ tons km}^{-2} \text{ yr}^{-1}$). Although the climatic and geological context of the southern Cascades differs appreciably from the central Andes, the erosion rates determined in this study fall well within the Andean range.

A rigorous topographic reconstruction of the study watersheds is beyond the scope of this report, however a simplistic analysis is informative. For example, consider the portion of Judd Creek below the meadow. Here, the elevation difference between the channel and the top of the interfluvium is about 40 m. If the watershed cross-sectional geometry is approximated as a "V", this implies a watershed average of 20 m of denudation since the rock was deposited at ca. 2 Ma, or about 10 m/m.y. Assuming an andesite density of 2.5 g cm^{-3} , this is equivalent to a watershed averaged denudation rate of $25 \text{ tons km}^{-2} \text{ yr}^{-1}$ and consistent with the measured ^{36}Cl erosion rate. Although the transient nature of volcanic landscapes, which degrade from an initial topographic form, suggest that erosion rates from volcanic reconstructions integrating over the whole history of the volcano may not be strictly comparable to 10 k.y. timescale erosion rates from cosmogenic nuclides,

the good agreement between the two methods at Judd Creek suggest that the ^{36}Cl erosion rates are robust.

7. CONCLUSIONS

In this study, long-term erosion rates were determined using cosmogenic ^{36}Cl in magnetite from stream sediment at nine forested watersheds in the Greater Battle Creek area. Erosion rates are lowest along Judd Creek (18-47 tons km^{-2} yr^{-1} decay corrected) and somewhat higher in the rest of the Greater Battle Creek watersheds (46-58 tons km^{-2} yr^{-1} decay corrected). Erosion-rate-averaging timescales range from 25,300 years to 72,800 years. These long-averaging timescales ensure that the erosion signal is unaffected by land use, although it may in part record long-term changes in erosion rate due to glacial-interglacial climate fluctuation (Schaller et al., 2001). Finally, it is worth noting that the measurement reproducibility of cosmogenic erosion rates is almost always greater than the analytical uncertainty due to the stochastic nature of erosional processes (Kober et al., 2012). Inter-sample variability in small watersheds under (100 km^2 in area) is typically ~15-25% (Foster and Anderson, 2016; Granger and Riebe, 2014; Moore, 2017). For this reason, a conservative estimate of the true uncertainty on the ^{36}Cl erosion rates may be closer to 25%. Nevertheless, these data should serve as a useful benchmark for evaluation of modern sediment yields.

8. REFERENCES

Bierman, P.R., Reuter, J.M., Pavich, M., Gellis, A.C., Caffee, M.W., Larsen, J., 2005. Using cosmogenic nuclides to contrast rates of erosion and sediment yield in a semi-arid, arroyo-dominated landscape, Rio Puerco Basin, New Mexico. *Earth Surf. Process. Landf.* 30, 935–953. doi:10.1002/esp.1255

Brown, E.T., Stallard, R.F., Larsen, M.C., Bourlès, D.L., Raisbeck, G.M., Yiou, F., 1998. Determination of predevelopment denudation rates of an agricultural watershed (Cayaguás River, Puerto Rico) using in-situ-produced ^{10}Be in river-borne quartz. *Earth Planet. Sci. Lett.* 160, 723–728. doi:10.1016/S0012-821X(98)00123-X

Carretier, S., Regard, V., Vassallo, R., Martinod, J., Christophoul, F., Gayer, E., Audin, L., Lagane, C., 2015. A note on ^{10}Be -derived mean erosion rates in catchments with heterogeneous lithology:

examples from the western Central Andes. *Earth Surf. Process. Landf.* 40, 1719–1729.
doi:10.1002/esp.3748

Clynne, M.A., Muffler, L.J.P., 2010. Geologic map of Lassen Volcanic National Park and vicinity, California. US Department of the Interior, US Geological Survey.

Covault, J.A., Craddock, W.H., Romans, B.W., Fildani, A., Gosai, M., 2013. Spatial and Temporal Variations in Landscape Evolution: Historic and Longer-Term Sediment Flux through Global Catchments. *J. Geol.* 121, 35–56. doi:10.1086/668680

Ferrier, K.L., Kirchner, J.W., Finkel, R.C., 2005. Erosion rates over millennial and decadal timescales at Caspar Creek and Redwood Creek, Northern California Coast Ranges. *Earth Surf. Process. Landf.* 30, 1025–1038.

Ferrier, K.L., Perron, J.T., Mukhopadhyay, S., Rosener, M., Stock, J.D., Huppert, K.L., Slosberg, M., 2013. Covariation of climate and long-term erosion rates across a steep rainfall gradient on the Hawaiian island of Kaua'i. *GSA Bull.* 125, 1146–1163. doi:10.1130/B30726.1

Foster, M.A., Anderson, R.S., 2016. Assessing the effect of a major storm on 10BE concentrations and inferred basin-averaged denudation rates. *Quat. Geochronol.* 34, 58–68.
doi:10.1016/j.quageo.2016.03.006

Granger, D.E., Kirchner, J.W., Finkel, R., 1996. Spatially Averaged Long-Term Erosion Rates Measured from in Situ-Produced Cosmogenic Nuclides in Alluvial Sediment. *J. Geol.* 104, 249–257.

Granger, D. E., and Riebe, C. S., 2014. Cosmogenic nuclides in weathering and erosion, in Drever, J. I., ed., *Surface and Ground Water, Weathering and Soils*, Volume 5 in Turekian, K. K., and Holland, H.D., eds., *Treatise on Geochemistry*, Elsevier-Pergamon, Oxford

Jennings, C.W., Strand, R.G., Rogers, T.H., Boylaw, R.T., 1977. Geologic map of California. Division of Mines and Geology.

Karátson, D., Telbisz, T., Wörner, G., 2012. Erosion rates and erosion patterns of Neogene to

Quaternary stratovolcanoes in the Western Cordillera of the Central Andes: An SRTM DEM based analysis. *Geomorphology* 139–140, 122–135. doi:10.1016/j.geomorph.2011.10.010

Kirchner, J.W., Finkel, R.C., Riebe, C.S., Granger, D.E., Clayton, J.L., King, J.G., Megahan, W.F., 2001. Mountain erosion over 10 yr, 10 k.y., and 10 m.y. time scales. *Geology* 29, 591–594. doi:10.1130/0091-7613(2001)029<0591:MEOYKY>2.0.CO;2

Kober, F., Hippe, K., Salcher, B., Ivy-Ochs, S., Kubik, P.W., Wacker, L., Hählen, N., 2012. Debris-flow-dependent variation of cosmogenically derived catchment-wide denudation rates. *Geology* 40, 935–938.

Lal, D., 1991. Cosmic ray labeling of erosion surfaces: in situ nuclide production rates and erosion models. *Earth Planet. Sci. Lett.* 104, 424–439. doi:10.1016/0012-821X(91)90220-C

Liu, B., Phillips, F.M., Fabryka-Martin, J.T., Fowler, M.M., Stone, W.D., 1994. Cosmogenic ^{36}Cl accumulation in unstable landforms: 1. Effects of the thermal neutron distribution. *Water Resour. Res.* 30, 3115–3125. doi:10.1029/94WR00761

Marrero, S.M., Phillips, F.M., Caffee, M.W., Gosse, J.C., 2015. CRONUS-Earth cosmogenic ^{36}Cl calibration. *Quat. Geochronol.* doi:10.1016/j.quageo.2015.10.002

Masarik, J., 2002. Numerical simulation of in situ production of cosmogenic nuclides.

Moore, A., 2017. Cosmogenic Be-10 and Cl-36 in magnetite (Master's Thesis in prep). Purdue University, W. Lafayette, IN.

Norton, K.P., von Blanckenburg, F., Kubik, P.W., 2010. Cosmogenic nuclide-derived rates of diffusive and episodic erosion in the glacially sculpted upper Rhone Valley, Swiss Alps. *Earth Surf. Process. Landf.* 35, 651–662. doi:10.1002/esp.1961

Parker, R.L., 1967. Data of geochemistry: composition of the earth's crust.

Phillips, F.M., 2016. Cosmogenic nuclide data sets from the Sierra Nevada, California, for assessment

of nuclide production models: I. Late Pleistocene glacial chronology. *Quat. Geochronol.*
doi:10.1016/j.quageo.2015.12.003

Phillips, F.M., Stone, W.D., Fabryka-Martin, J.T., 2001. An improved approach to calculating low-energy cosmic-ray neutron fluxes near the land/atmosphere interface. *Chem. Geol.* 175, 689–701.
doi:10.1016/S0009-2541(00)00329-6

Reusser, L., Bierman, P., Rood, D., 2015. Quantifying human impacts on rates of erosion and sediment transport at a landscape scale. *Geology* 43, 171–174. doi:10.1130/G36272.1

Ruxton, B.P., McDougall, I., 1967. Denudation rates in northeast Papua from potassium-argon dating of lavas. *Am. J. Sci.* 265, 545–561. doi:10.2475/ajs.265.7.545

Safran, E.B., Bierman, P.R., Aalto, R., Dunne, T., Whipple, K.X., Caffee, M., 2005. Erosion rates driven by channel network incision in the Bolivian Andes. *Earth Surf. Process. Landf.* 30, 1007–1024.
doi:10.1002/esp.1259

Schaller, M., von Blanckenburg, F., Hovius, N., Kubik, P.W., 2001. Large-scale erosion rates from in situ-produced cosmogenic nuclides in European river sediments. *Earth Planet. Sci. Lett.* 188, 441–458. doi:10.1016/S0012-821X(01)00320-X

Shacklette, H.T., Boerngen, J.G., 1984. Element concentrations in soils and other surficial materials of the conterminous United States.

Wittmann, H., von Blanckenburg, F., Kruesmann, T., Norton, K.P., Kubik, P.W., 2007. Relation between rock uplift and denudation from cosmogenic nuclides in river sediment in the Central Alps of Switzerland. *J. Geophys. Res. Earth Surf.* 112, F04010. doi:10.1029/2006JF000729